CHEMISTRY
A EUROPEAN JOURNAL

DOI: 10.1002/chem.200902834

Highly Uniform YBO_3 Hierarchical Architectures: Facile Synthesis and Tunable Luminescence Properties

Guang Jia, Hongpeng You,* Kai Liu, Yuhua Zheng, Ning Guo, Junjiao Jia, and Hongjie Zhang*[a]

Abstract: Highly uniform pancake-like YBO_3 hierarchical architectures have been successfully prepared by a designed two-step hydrothermal method. Yttrium precursor microprisms were first synthesized according to a simple hydrothermal route. Subsequently, nearly monodisperse multilayered YBO_3 products with a pancake-like shape were synthesized at the expense of the precursor during the hydrothermal process. The whole process was carried out under aqueous conditions without the use of any organic solvent, surfactant, or catalyst. The conversion process from the precursor to YBO_3 products has been investigated by time-dependent XRD experiments. Extending this method, other $LnBO_3$ (Ln = Ho, Er, Tm, Yb) samples with well-defined shape and dimensionality have also been obtained by a similar synthetic process. The luminescence colors of YBO_3 samples co-doped with Eu^{3+} and Tb^{3+} under ultraviolet or low-voltage electron beam excitation can be tuned from red, through yellow and green-yellow, to green by simply adjusting the relative doping concentrations of the activator ions. This merit of multicolor emissions in the visible region endows materials of this kind with potential application in the fields of light-display systems and optoelectronic devices.

Keywords: chemical conversion · hierarchical architectures · hydrothermal synthesis · luminescence · yttrium orthoborate

Introduction

In recent years, the synthesis of inorganic nano-/micromaterials with well-defined and controllable morphologies has attracted considerable attention, because the properties of such materials are closely related to geometrical factors such as morphology, dimensionality, and size.[1–6] In particular, the fabrication of hierarchical and complex nano-/microstructures by the assembly of nanoparticles, nanorods, nanosheets, or nanobelts as building blocks at different levels has recently been proposed and partially realized.[7–11] To date, a variety of materials, such as oxides,[12–14] sulfides,[15,16] hydrates,[17,18] and other compounds,[19–23] have been prepared with controlled hierarchical/complex morphologies by various methods. In these fabrications, the hydrothermal method, as a typical solution-based approach, has proved to be an effective and convenient synthesis technique for preparing various inorganic materials with diverse morphologies and architectures. During the hydrothermal process, complexing agents or surfactants always play an important role in controlling the dynamics of crystal growth and determining the final morphology of the hierarchical nano-/microstructures.[22–24] However, the addition of complexing agents or surfactants usually involves a complicated process and incurs a high cost, and may result in impurities in the products. Therefore, it is desirable to develop environmentally friendly, facile, and low-cost methods for the fabrication of uniform inorganic hierarchical architectures without any organic solvent, catalyst, or surfactant.

Recently, much research effort has been directed towards the synthesis of rare-earth compounds since they can be used as highly efficient phosphors, catalysts, and other functional materials by virtue of their novel optical, electronic, and chemical properties.[25–29] In particular, rare-earth orthoborates have proved to be very useful host lattices for lumi-

[a] Dr. G. Jia, Prof. H. You, K. Liu, Y. Zheng, N. Guo, J. Jia, Prof. H. Zhang
State Key Laboratory of Rare Earth Resource Utilization
Changchun Institute of Applied Chemistry
Chinese Academy of Sciences, Changchun 130022 (PR China)
and
Graduate University of the Chinese Academy of Sciences
Beijing 100049 (PR China)
Fax: (+86) 431-8569-8041
E-mail: hpyou@ciac.jl.cn
hongjie@ciac.jl.cn

Supporting information for this article is available on the WWW under http://dx.doi.org/10.1002/chem.200902834.

nescence, and have found widespread application in mercury-free fluorescent lamps and various kinds of display devices.[30–32] For instance, yttrium orthoborate (YBO_3) has attracted much attention because of its low toxicity, strong luminescence intensity, high chemical stability, and exceptional optical damage threshold.[33,34] To date, various morphologies of YBO_3 have been synthesized according to different methods, such as well-dispersed nanocrystals,[33,34] one-dimensional (1D) nanowires and nanotubes,[37] drum-like microcrystals,[38] 3D flower-like architectures,[39] and core–shell structures.[40] To the best of our knowledge, there have been few reports on the synthesis of multilayered YBO_3 microstructures with a uniform pancake-like shape. Among the lanthanide ions, Eu^{3+} and Tb^{3+} ions are two of the most important luminescent centers, which have been regarded as attractive for use as visible luminescent materials because of their strong red and green emissions. As is well known, YBO_3 has also proved to be a very useful host lattice for the luminescence of Eu^{3+} and Tb^{3+} ions.[31,35–42] However, to the best of our knowledge, little attention has been paid to the tunable luminescence properties of Eu^{3+}- and Tb^{3+}-codoped YBO_3 phosphors.

In the work described in this paper, uniform and well-dispersed pancake-like YBO_3 hierarchical architectures have been successfully prepared through a hydrothermal conversion approach, without the use of any organic solvent or surfactant. Their structure, morphology, formation process, and luminescence properties have been investigated in detail. Moreover, it is interesting to note that other rare-earth orthoborates, $LnBO_3$ (Ln = Ho, Er, Tm, Yb), which have similar morphologies as the as-synthesized YBO_3 sample, could also be successfully prepared by this general and facile chemical conversion route.

Results and Discussion

Phase identification, morphology, and formation process of YBO_3 hierarchical architectures: Figure 1a shows the X-ray diffraction pattern of the as-formed yttrium precursor. It can be seen that all diffraction peaks of the precursor can be readily indexed to the monoclinic phase of $Y_4O(OH)_9NO_3$ (JCPDS no. 79-1352).[43] In order to understand the formation process of the YBO_3 samples, time-dependent XRD experiments were performed (2:1 molar ratio of H_3BO_3/precursor). When the reaction was carried out at 180 °C for 1 h, the diffraction peaks of the product showed no obvious change in comparison with those of the precursor (Figure 1b). On increasing the reaction time to 3 h (Figure 1c), it can be seen that the diffraction peaks of the precursor had nearly disappeared, and that intense peaks due to the hexagonal $Y(OH)_3$ phase had developed (labeled in Figure 1c). This indicates that most of the $Y_4O(OH)_9NO_3$ precursor had been transformed to more stable hexagonal $Y(OH)_3$ during the hydrothermal process. Meanwhile, some weak diffraction peaks due to the hexagonal YBO_3 phase (JCPDS no. 16-0277) could also be observed at this stage. On extending the reaction time to 4 h or longer, both the residual $Y_4O(OH)_9NO_3$ and $Y(OH)_3$ phases had completely disappeared, having been converted to the pure hexagonal YBO_3 phase (Figures 1d, e). The XRD results presented above agree well with the corresponding SEM observations (see Figures 3 and 4). In addition, the diffraction peaks of the as-obtained YBO_3 samples were very sharp and strong, indicating that products with high crystallinity could be prepared by this conversion method. This is important for phosphors, because high crystallinity generally means fewer traps and stronger luminescence.

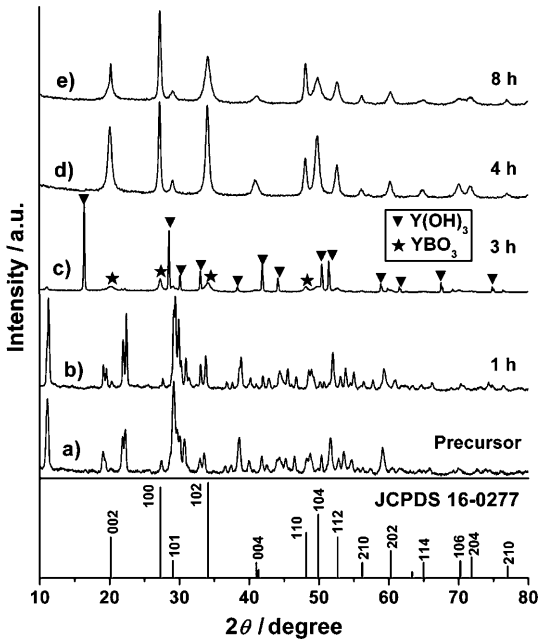

Figure 1. XRD patterns of a) the yttrium precursor, and the hydrothermal conversion products prepared at 180 °C for b) 1 h, c) 3 h, d) 4 h, and e) 8 h, along with the standard data for hexagonal-phase YBO_3 (JCPDS no. 16-0277) as a reference.

Figure 2a shows the FT-IR spectrum of the as-obtained yttrium precursor. The IR bands in the range 3400–3700 cm^{-1} can be attributed to symmetrical and asymmetrical stretching vibrations of O–H groups, thus confirming the presence of OH^- in the precursor. The peaks at about 693, 828, 1060, 1366, and 1408 cm^{-1} can be attributed to bending and stretching vibrations of NO, NO_2, and NO_3 groups, confirming the presence of NO_3^-. The band centered at 533 cm^{-1} is characteristic of Y–O stretching vibrations.[44] The results further support the structural formula $[Y_4O(OH)_9(NO_3)]$ of the precursor. Figure 2b shows the FT-IR spectrum of the YBO_3 sample prepared at 180 °C for 4 h. It is clear that the characteristic bands of the NO_3^- and OH^- groups of the precursor are no longer seen after the hydrothermal process. Instead, some intense bands appear in the range 800–1200 cm^{-1} (centered at 847, 905, and 1153 cm^{-1}) (Figure 2b), which can be assigned as the characteristic bands of vaterite-type orthoborates.[42,45,46] Trivalent lanthanide orthobo-

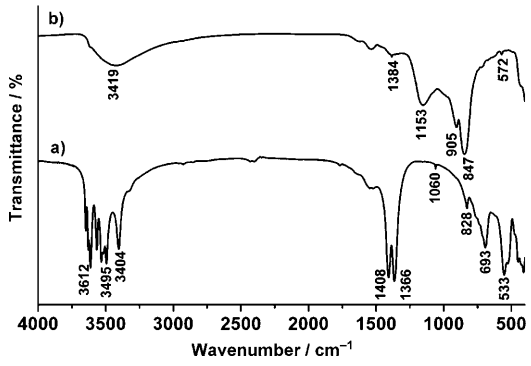

Figure 2. FT-IR spectra of a) the yttrium precursor and b) the YBO_3 product prepared at 180 °C for 4 h.

rates are isostructural with one of the three forms of calcite, aragonite, or vaterite. The vibrational spectra of vaterite-type orthoborates are found to be markedly different from those of calcite- and aragonite-type orthoborates. Specifically, a group of bands in the region 800–1200 cm^{-1} is seen in the spectra of vaterite-type orthoborates.[42] The intense absorption bands in the range 800–1200 cm^{-1} can be ascribed to the vibrational modes of the $B_3O_9^{9-}$ group in vaterite-type orthoborates.[33,47] The IR absorption bands at 847 and 905 cm^{-1} are assigned to ring-stretching vibration modes, while that at 1153 cm^{-1} is assigned to a terminal stretching vibration mode.[36,47] A band at 1346 cm^{-1} is due to an asymmetric stretching vibration of the BO_3 group. There are some weak absorption bands in the range 1250–1600 cm^{-1}, which may originate from the $(BO_4)^{5-}$ group present in the small amount of Y_3BO_6 phase.[37] In addition, a small peak near 572 cm^{-1} can be assigned to an in-plane bending of the BO_4 group or the BO_3 group in vaterite-type orthoborates.[45,46] The results provide additional evidence that the precursor had been largely converted to a vaterite-type YBO_3 phase after the hydrothermal process.

A series of parallel experiments with different molar ratios of H_3BO_3/precursor (1.5:1, 3:1, 5:1) was performed at 180 °C for 4 h. The XRD patterns revealed that the samples prepared with different molar ratios of H_3BO_3/precursor exhibited identical diffraction peaks, which could be readily indexed to the pure hexagonal phase of YBO_3 (see Figure S1 in the Supporting Information). No impurity peaks were observed, indicating the high purity of the products. As can be seen from the corresponding FT-IR spectra (Figure S2 in the Supporting Information), the absorption bands of the as-synthesized samples can be assigned as the characteristic bands of vaterite-type orthoborates, and are identical to those of the YBO_3 sample obtained with a 2:1 molar ratio of H_3BO_3/precursor (Figure 2b). The XRD and FT-IR results indicate that the precursor can be easily and completely converted to vaterite-type YBO_3 when H_3BO_3 is in excess with respect to the precursor after the hydrothermal treatment. The YBO_3 sample prepared from a 2:1 molar ratio of H_3BO_3/precursor was utilized to investigate the morphology, formation process, and tunable luminescence properties.

Figure 3a shows an SEM image of the as-formed yttrium precursor, which clearly indicates that the $Y_4O(OH)_9NO_3$ precursor is entirely comprised of microprisms with diameters of 1.5–2 μm and lengths of about 10 μm. It can also be observed that the microprisms are well-dispersed and have a narrow size distribution. After these microprisms had reacted with H_3BO_3 at 180 °C for 4 h, uniform and well-dispersed pancake-like YBO_3 hierarchical structures were obtained on a large scale (Figure 3b). It can also be observed that each YBO_3 "pancake" has a concave dip at its centre, and that the average size of the as-prepared product is 3–4 μm in diameter and about 1.5 μm in thickness. As can be seen from the enlarged SEM image (Figure 3c), the rough surface and evident boundaries of the pancake-like forms indicate that an individual YBO_3 "pancake" is composed of many thinner microsheets, which are integrated along the longitudinal axis direction through face-to-face attachment. A TEM image further confirmed the size and perfect round shape of the YBO_3 sample (Figure 3d), in good agreement with the SEM observations. The selected-area electron diffraction (SAED) pattern (inset in Figure 3d) obtained from a single YBO_3 "pancake" shows regular diffraction spots and confirms the single-crystalline nature of the YBO_3 sample.

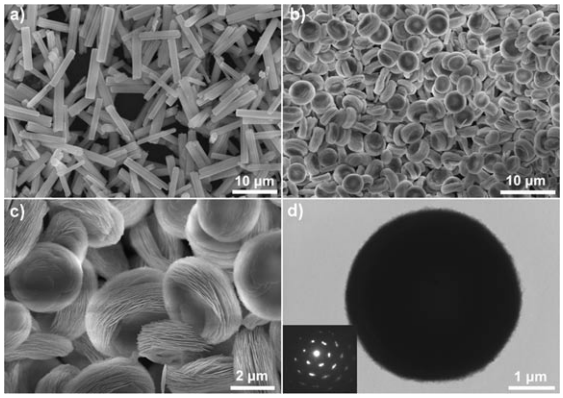

Figure 3. a) SEM image of the $Y_4O(OH)_9NO_3$ precursor; b, c) SEM and d) TEM images of the YBO_3 sample prepared at 180 °C for 4 h. The inset in d) is the corresponding SAED pattern taken from a single microstructure.

To understand the detailed conversion process of the YBO_3 hierarchical architecture, SEM images of the conversion products prepared at 180 °C for different times were acquired (Figure 4). When the reaction was carried out at 180 °C for 1 h, it can be seen that some nanoplates formed besides the microprisms (Figure 4a). On increasing the reaction time to 3 h, a large amount of pancake-like microstructures promptly appeared (Figure 4b), indicating that the renucleation and crystal growth process of the YBO_3 sample was very fast. At the same time, it can also be seen that both the quantity and size of the precursor microprisms decreased. When the reaction time was extended to 4 h, the microprisms and nanoplates disappeared completely, having been transformed to pure multilayered YBO_3 architectures

(Figure 3). On extending the reaction time to 8 h, the as-obtained multilayered YBO_3 micropancakes showed no obvious morphological change in comparison to the sample prepared for 4 h (Figure 4c). However, after a further increase in the reaction time to 12 h, some spherical and flower-like microstructures assembled from densely packed microsheets could clearly be observed besides the multilayered micropancakes (Figure 4d). The inset in Figure 4d shows a typical high-magnification SEM image of a single spherical hierarchical microstructure.

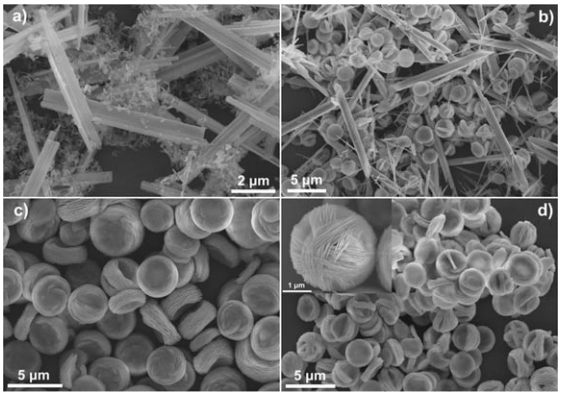

Figure 4. SEM images of the hydrothermal conversion products prepared at 180 °C for a) 1 h, b) 3 h, c) 8 h, and d) 12 h. The inset in d) is the enlarged SEM image of a single spherical hierarchical microstructure.

On the basis of the above XRD and SEM results and analysis, the possible conversion process may be as follows. In the early stages of the reaction, the microprism precursor dissolves in the solution and generates Y^{3+} ions under the hydrothermal conditions. With the increase of reaction time, the H_3BO_3 is able to react with Y^{3+} to form some YBO_3 nanoplates. Subsequently, these nanoplates grow anisotropically to form pancake-like multilayered structures in a short time. Meanwhile, most of the $Y_4O(OH)_9NO_3$ precursor is transformed to more stable $Y(OH)_3$ during the hydrothermal process (Figure 1c). As the reaction proceeds, the $Y_4O(OH)_9NO_3$ and $Y(OH)_3$ precursors are completely consumed, being converted into uniform and well-dispersed pancake-like YBO_3 hierarchical architectures. The conversion process is completed in a very short time. After further hydrothermal treatment, some multilayered micropancakes undergo a further crystal growth and crystallization process driven by minimization of the total surface energy of the system, giving rise to the formation of complex spherical or flower-like microstructures.[47] A schematic illustration of the overall formation process of YBO_3 hierarchical architectures is presented in Scheme 1, and the main chemical reactions can be written as follows:

$$4Y^{3+} + NO_3^- + 11NH_3 \cdot H_2O \rightarrow Y_4O(OH)_9NO_3 + 11NH_4^+ + H_2O$$

$$Y_4O(OH)_9NO_3 + OH^- + H_2O \rightarrow 4Y(OH)_3 + NO_3^-$$

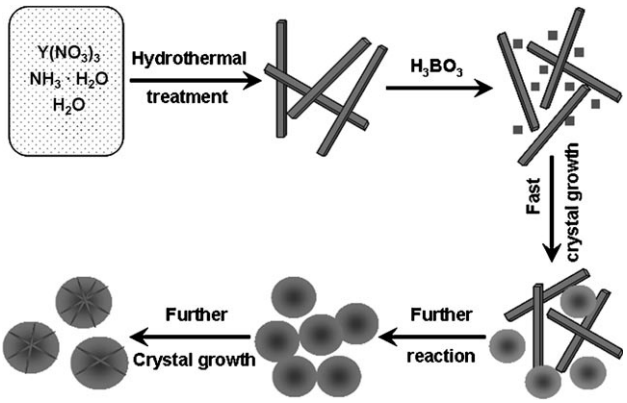

Scheme 1. Schematic illustration of the formation process of YBO_3 hierarchical architectures.

$$Y(OH)_3 + H_3BO_3 \rightarrow YBO_3 + 3H_2O$$

Luminescence properties of Eu^{3+}- and Tb^{3+}-doped YBO_3 samples: The photoluminescence (PL) properties of Eu^{3+}- and Tb^{3+}-doped YBO_3 samples (180 °C, 4 h) were investigated. The excitation spectrum of a YBO_3/5 % Eu^{3+} sample consists of a strong absorption band centered at 245 nm and some weak lines, which can be assigned to the charge-transfer band between the O^{2-} and Eu^{3+} ions and the f-f transitions of the Eu^{3+} ions, respectively (Figure 5a). Upon excitation at 245 nm, the emission spectrum of YBO_3/5 % Eu^{3+} consists of a group of lines at about 578, 591, 610 (626), 649, and 706 nm, which can be attributed to $^5D_0$–^7F_J ($J=0$, 1, 2, 3, 4) transition lines of the Eu^{3+} ions, respectively (Figure 5b). The $^5D_0$–$^7F_1$ transition has generally proved to be the dominant emission peak of Eu^{3+} in many previously reported YBO_3/Eu^{3+} systems,[35–38,40] application of which has always been restricted by its relatively poor chromaticity. For comparison, the emission spectrum of a bulk YBO_3/5 % Eu^{3+} sample prepared by solid-state reaction (SSR) is shown in Figure 5e. It can clearly be seen that the main peak positions in the emission spectra of the two samples are identical, but that the relative intensities of the $^5D_0$–$^7F_1$ and $^5D_0$–$^7F_2$ transitions of the Eu^{3+} ions differ to some extent. The YBO_3/5 % Eu^{3+} sample prepared by the hydrothermal conversion method showed better chromaticity compared to that of the bulk sample, which could be confirmed by the CIE (Commission Internationale de l'Éclairage, 1931) chromaticity diagram (see points a and f in Figure S3 in the Supporting Information). The improvement in color chromaticity can be attributed to the distinct multilayered microstructure of the YBO_3/Eu^{3+} sample. The multilayered hierarchical architectures possess especially large surface areas and high surface energies, which not only provide a driving force for the self-assembly, but also result in a high degree of disorder near the surface and corresponding lower symmetry of the crystal field around the Eu^{3+} ions than in the bulk materials.[22,38] According to the Judd–Ofelt theory,[48] a lower symmetry of the crystal field around the Eu^{3+} ions would result in a higher R/O value

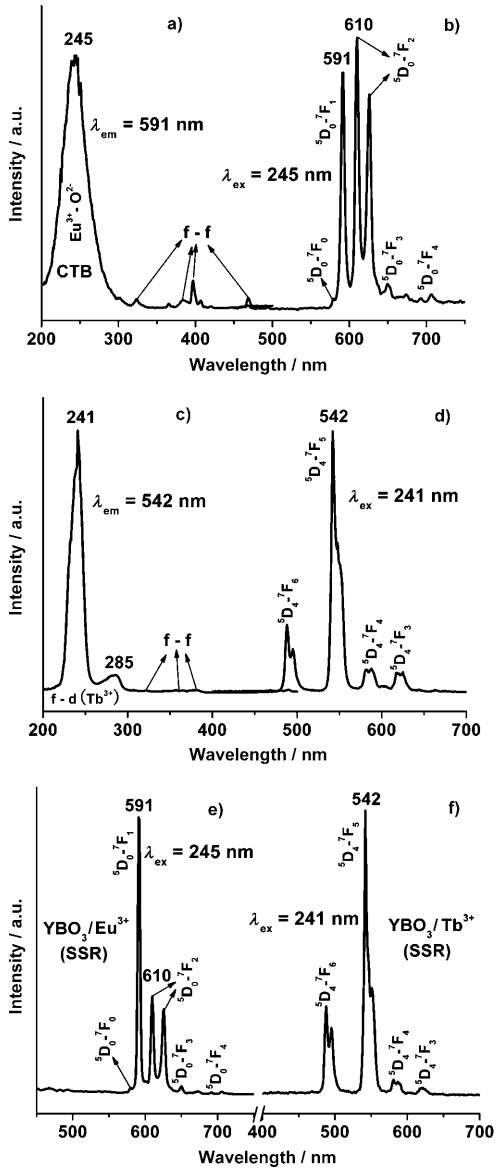

Figure 5. PL excitation and emission spectra of YBO_3/5% Eu^{3+} (a, b) and YBO_3/5% Tb^{3+} (c, d) samples prepared at 180°C for 4 h; and emission spectra of bulk YBO_3/5% Eu^{3+} (e) and YBO_3/5% Tb^{3+} (f) samples prepared by solid-state reaction (SSR).

(R = red, $^5D_0$–$^7F_2$; O = orange, $^5D_0$–$^7F_1$) and a better color chromaticity.

The excitation spectrum of a YBO_3/5% Tb^{3+} sample is composed of two intense bands and some weak lines (Figure 5c). The intense bands centered at 241 and 285 nm can be attributed to the spin-allowed transition ($\Delta S = 0$) with higher energy and the spin-forbidden transition ($\Delta S = 1$) with lower energy from the 4f to the 5d level of the Tb^{3+} ions.[45,46] The other weak lines are due to the characteristic f-f transitions of the Tb^{3+} ions. The emission spectrum consists of a group of lines centered at about 488, 542, 587, and 624 nm, which correspond to the $^5D_4$–^7F_J ($J = 6, 5, 4, 3$) transitions of the Tb^{3+} ions, respectively (Figure 5d). By comparison with the emission spectrum of YBO_3/5% Tb^{3+} prepared by the solid-state reaction (Figure 5f), it can be seen that the two emission spectra are essentially identical. It is well known that Tb^{3+} ions can be easily oxidized during a calcination process in air, hence Tb^{3+}-doped YBO_3 should be synthesized in a reducing atmosphere at high temperature, which involves a complicated reaction process. In this case, however, the green-emitting YBO_3/Tb^{3+} phosphor could be prepared by the hydrothermal conversion method without a reducing atmosphere.

In order to investigate the tunable PL properties of the YBO_3 samples, we co-doped the YBO_3 host lattice with different relative concentrations of Eu^{3+} and Tb^{3+} ions (total dopant concentration: 5 mol%). Figure 6 shows the PL emission spectra of the Eu^{3+}- and Tb^{3+}-co-doped YBO_3 samples under excitation at 241 nm. It can be seen that the as-obtained purely Eu^{3+}-doped YBO_3 sample showed strong red emission under excitation with UV light. By co-doping the YBO_3 host lattice with Tb^{3+} ions, the characteristic emission of the Tb^{3+} ions could be observed besides the Eu^{3+} emission. As one might expect, on increasing the relative concentration ratio of Tb^{3+}/Eu^{3+}, the luminescence of the Eu^{3+} ions gradually decreased, while that of Tb^{3+} increased. Finally, the purely Tb^{3+}-doped YBO_3 sample showed bright-green emission. As a result, the photoluminescence color can be tuned from red, through yellow and green-yellow, to green by simply adjusting the relative doping concentrations of the Tb^{3+} and Eu^{3+} ions. This result was confirmed by the corresponding CIE chromaticity diagram for the emission spectra of the Eu^{3+}- and Tb^{3+}-co-doped YBO_3 samples (see points a–e in Figure S3 in the Supporting Information). It indicates that the as-obtained phosphors were capable of showing multicolor emissions in the visible region under single-wavelength excitation, a merit that might make them amenable to potential applications in fields such as light-display systems and optoelectron-

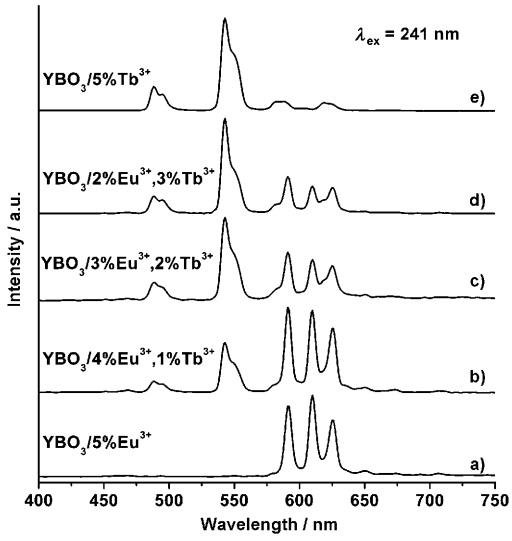

Figure 6. PL emission spectra of the Eu^{3+}- and Tb^{3+}-co-doped YBO_3 samples under excitation at 241 nm (total dopant concentration: 5 mol%).

ic devices. It is important to note that the bulk Eu^{3+}- and Tb^{3+}-doped YBO_3 phosphors were synthesized under different atmospheres at high temperature (YBO_3/Eu^{3+} in air; YBO_3/Tb^{3+} in a reducing atmosphere), hence it would be difficult to prepare Eu^{3+}- and Tb^{3+}-co-doped YBO_3 samples with tunable luminescence properties by a traditional solid-state reaction.

Figure 7 shows the PL decay curves for the luminescence of the YBO_3/5% Eu^{3+} (591 nm, $^5D_0$–$^7F_1$) and YBO_3/5% Tb^{3+} (542 nm, $^5D_4$–$^7F_5$) samples, respectively. It can be seen that both decay curves can be well fitted by a single-exponential function of the form $I(t)=I_0 \exp(-t/\tau)$ (where I_0 is the initial emission intensity at $t=0$ and τ is the 1/e lifetime of the emissive center). In this way, the lifetimes were determined as 1.827 and 3.161 ms for the YBO_3/5% Eu^{3+} and YBO_3/5% Tb^{3+} samples, respectively.

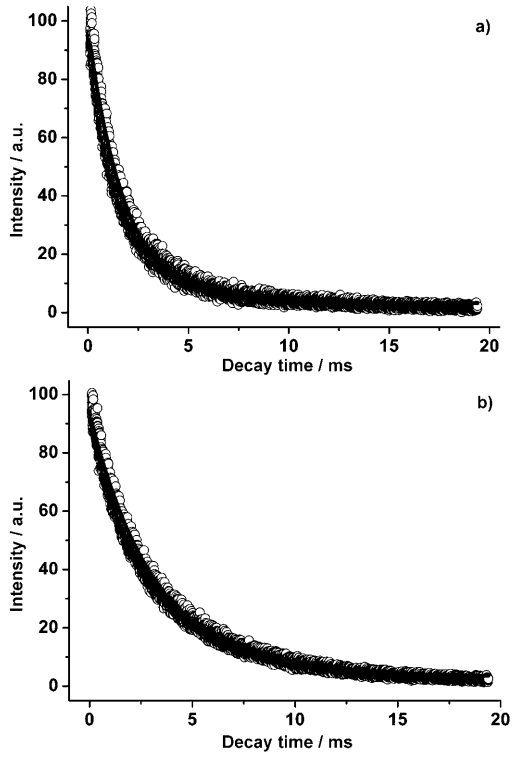

Figure 7. Decay curves for the as-prepared samples (○: experimental data, ●: fitted by $I = A\exp(-t/\tau)$): a) YBO_3/5% Eu^{3+} ($\lambda=591$ nm, $^5D_0$–$^7F_1$, $\tau = 1.827$ ms) and b) YBO_3/5% Tb^{3+} ($\lambda=542$ nm, $^5D_4$–$^7F_5$, $\tau = 3.161$ ms).

The cathodoluminescence (CL) properties of the as-prepared YBO_3/5% Eu^{3+} and YBO_3/5% Tb^{3+} samples were also investigated. Figure 8 shows typical CL spectra of YBO_3/5% Eu^{3+} and YBO_3/5% Tb^{3+} samples under excitation with an electron beam (accelerating voltage: 3.5 kV; filament current: 98 mA). It can be observed that the Eu^{3+}- and Tb^{3+}-doped YBO_3 phosphors show strong red and green emissions under the excitation of a low-voltage electron beam, and that the CL spectra are essentially identical to the corresponding PL emission spectra (Figure 5). However, the relative intensities of the emission peaks in the PL and CL spectra are seen to vary, which may be caused by the different excitation mechanisms.[49,50] The Eu^{3+}- and Tb^{3+}-co-doped YBO_3 samples produced bright-yellow and green-yellow emissions under the excitation of a low-voltage electron beam, which were similar to those of the purely Eu^{3+}- or Tb^{3+}-doped YBO_3 samples (not shown here). Furthermore, the CL emission intensities of the YBO_3/5% Eu^{3+} and YBO_3/5% Tb^{3+} samples were studied as a function of accelerating voltage and filament current. It was found that the CL intensity increased markedly with increasing accelerating voltage or filament current (see Figure S4 in the Supporting Information). The increase in CL brightness with an increase in electron energy or filament current can be attributed to deeper penetration of electrons into the body of the phosphor and the larger electron beam current density.[40,44,51] The electron penetration depth can be estimated from the empirical formula L [Å] $=250(A/\rho)(E/Z^{1/2})^n$, where $n=1.2/(1-0.29\log_{10}Z)$, A is the atomic weight, ρ is the density, Z is the atomic number, and E is the accelerating voltage (kV).[51] For cathodoluminescence, the Eu^{3+} and Tb^{3+} ions are excited by the plasma produced by the incident electrons. With the increase of accelerating voltage or filament current, more plasma will be produced by the incident electrons, resulting in more Eu^{3+} being excited and hence higher CL intensity. Due to their strong CL intensity at low voltage and excellent dispersing properties, the as-synthesized phosphors may be potentially applied in field-emission display devices.

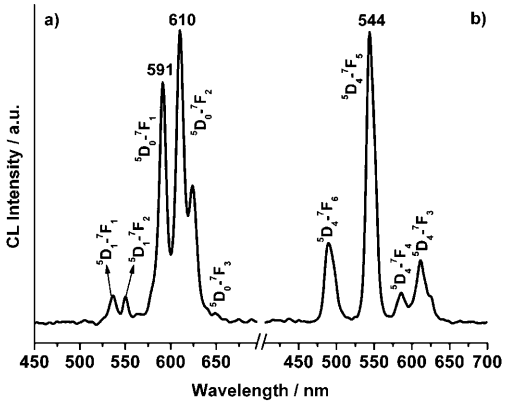

Figure 8. Typical cathodoluminescence spectra of a) YBO_3/5% Eu^{3+} and b) YBO_3/5% Tb^{3+} samples (accelerating voltage: 3.5 kV; filament current: 98 mA).

Synthesis of other lanthanide orthoborates $LnBO_3$ (Ln=Ho, Er, Tm, Yb): As is well known, lanthanide atoms and ions have similar ionic radii that vary only gradually across the series. As a result, lanthanide compounds may have similar physical and/or chemical properties.[28,52,53] In the present study, other lanthanide orthoborates $LnBO_3$ (Ln=Ho, Er, Tm, Yb) were also synthesized by the general method. As in the case of yttrium, the lanthanide precursors were first prepared by a simple hydrothermal process. It was apparent

from the XRD patterns that the diffraction peaks of the precursors could be readily indexed to the monoclinic phase of $Y_4O(OH)_9NO_3$, thus indicating that the as-formed precursors were also of the structure type $Ln_4O(OH)_9NO_3$ (see Figure S5 in the Supporting Information).[43,54] SEM images showed that the precursors were composed of one-dimensional microprisms or microrods, similar to those of the $Y_4O(OH)_9NO_3$ precursor (see Figure S6 in the Supporting Information). Upon reaction with H_3BO_3 under the designed hydrothermal conditions (2:1 molar ratio of H_3BO_3/lanthanide precursor), the precursors were converted to the pure hexagonal phases of $LnBO_3$ (Ln = Ho, Er, Tm, Yb) samples. This was confirmed by the XRD patterns of the hydrothermal conversion products (see Figure S7 in the Supporting Information). The morphologies of the as-obtained $LnBO_3$ samples were investigated by SEM (Figure 9). Generally, the morphologies of the as-obtained $LnBO_3$ samples were very similar to that of the as-synthesized YBO_3 sample (Figure 3). However, owing to the lanthanide contraction, a slight morphology variation among the different lanthanide orthoborates was evident. It can be concluded that various $LnBO_3$ samples with uniform hierarchical architectures could be synthesized by this simple and general conversion route. The formation processes of the $LnBO_3$ (Ln = Ho, Er, Tm, Yb) samples were essentially similar to that of the YBO_3 sample.

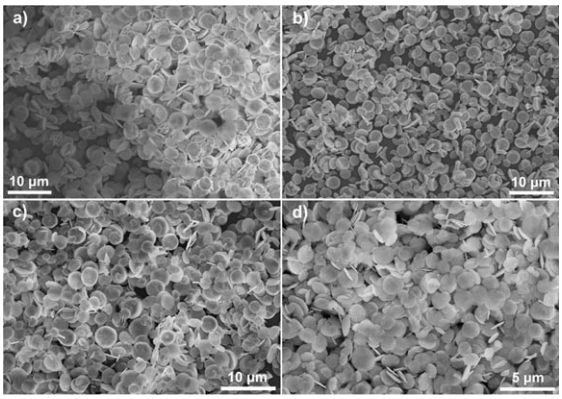

Figure 9. SEM images of as-obtained a) $HoBO_3$, b) $ErBO_3$, c) $TmBO_3$, and d) $YbBO_3$ samples.

Conclusion

In summary, we have demonstrated a general and facile hydrothermal conversion method for the synthesis of uniform and well-dispersed YBO_3 hierarchical architectures with pancake-like shapes. The crystal structure, morphology, and luminescence properties have been characterized by XRD/FT-IR, SEM/TEM, and PL, CL, and kinetic decays, respectively. The detailed conversion process from the precursor $Y_4O(OH)_9NO_3$ to the product YBO_3 has been investigated on the basis of time-dependent XRD experiments. Furthermore, it was interesting to find that the photoluminescence colors of the YBO_3 samples co-doped with Eu^{3+} and Tb^{3+} could be tuned from red, through yellow and green-yellow, to green by simply adjusting the relative doping concentrations of the activator ions. Furthermore, other $LnBO_3$ (Ln = Ho, Er, Tm, Yb) samples with well-defined morphologies and dimensionalities have also been synthesized by this hydrothermal conversion route, which indicates that this general, facile, and low-cost method may be more widely applicable in the design of other rare-earth compounds with well-defined hierarchical architectures.

Experimental Section

Aqueous solutions of $Ln(NO_3)_3$ (Ln = Y, Eu, Ho, Er, Tm, and Yb) and $Tb(NO_3)_3$ were obtained by dissolving Ln_2O_3 (99.99%) and Tb_4O_7 (99.99%) in dilute HNO_3 solution under heating with agitation.

Synthesis of the yttrium precursor: The yttrium precursor was prepared according to a previous report.[43] In a typical procedure, 1 M aqueous $Y(NO_3)_3$ solution (2 mL) was added to deionized water (35 mL). Then, 25 wt% aqueous ammonia solution was added to the solution until pH 11 was reached. After additional agitation for 30 min, the as-obtained white colloidal suspension was transferred to a 50 mL autoclave and heated at 200 °C for 24 h. The precursor was subsequently washed several times and redispersed in deionized water (10 mL).

Synthesis of YBO_3 samples: H_3BO_3 (0.13 g, 2 mmol) was first dissolved in deionized water (35 mL), and then 5 mL of the as-prepared precursor suspension was added with continuous stirring (2:1 molar ratio of H_3BO_3/precursor). After additional agitation for 30 min, the mixture was transferred to a 50 mL autoclave and maintained at 180 °C for 4 h. The white precipitate formed was washed with deionized water, collected by centrifugation, and dried at 60 °C in air.

A similar process was employed to prepare Eu^{3+}- and Tb^{3+}-doped YBO_3 samples, except that appropriate amounts of $Eu(NO_3)_3$ and $Tb(NO_3)_3$ were added to the aqueous solution of $Y(NO_3)_3$ at the initial stage. Additionally, different molar ratios (1.5:1, 3:1, and 5:1) of H_3BO_3/precursor and hydrothermal treatment times (1 h, 3 h, 8 h, 12 h, 180 °C) were selected to investigate the conversion process from the precursor to the final YBO_3 products.

For comparison, bulk YBO_3/Eu^{3+} and YBO_3/Tb^{3+} samples were prepared by a normal solid-state reaction (SSR) using stoichiometric amounts of Y_2O_3, Eu_2O_3, and Tb_4O_7 and excess H_3BO_3 at 1100 °C for 5 h. The YBO_3/Eu^{3+} sample was synthesized directly in air, whereas the YBO_3/Tb^{3+} sample was obtained under a reducing atmosphere of CO.

Synthesis of other $LnBO_3$ samples: Other $LnBO_3$ (Ln = Ho, Er, Tm, Yb) samples were prepared by a similar synthetic process using aqueous solutions of $Ho(NO_3)_3$, $Er(NO_3)_3$, $Tm(NO_3)_3$, or $Yb(NO_3)_3$ instead of $Y(NO_3)_3$ in the initial stage. The corresponding $LnBO_3$ samples were also prepared by the hydrothermal conversion route, maintaining the mixtures at 200 °C for 24 h (2:1 molar ratio of H_3BO_3/precursor).

Characterization: The samples were characterized by powder X-ray diffraction (XRD) performed on a D8 Focus diffractometer (Bruker). Fourier-transform infrared (FT-IR) spectra were measured with a Perkin–Elmer 580 B infrared spectrophotometer from samples in KBr pellets. The morphology of the samples was inspected using a scanning electron microscope (SEM; S-4800, Hitachi). Transmission electron microscopy (TEM) images and selected-area electron diffraction (SAED) patterns were obtained using a JEOL 2010 transmission electron microscope operating at 200 kV. Photoluminescence (PL) excitation and emission spectra were recorded with a Hitachi F-4500 spectrophotometer equipped with a 150 W xenon lamp as the excitation source. Cathodoluminescence (CL) measurements were carried out in an ultra-high-vacuum chamber ($<10^{-8}$ Torr), and the spectra were recorded on an F-4500 spectrophotometer. PL decay curves were obtained by means of a Lecroy Wave Runner 6100 digital oscilloscope (1 GHz) using a tunable laser (pulse

width = 4 ns, gate = 50 ns) as the excitation source (Continuum Sunlite OPO). All measurements were performed at room temperature.

Acknowledgements

This work has been financially supported by the National Natural Science Foundation of China (Grant No. 20771098), the Fund for Creative Research Groups (Grant No. 20921002), and the National Basic Research Program of China (973 Program, Grant Nos. 2007CB935502 and 2006CB601103).

[1] A. P. Alivisatos, *Science* **1996**, *271*, 933–937.
[2] C. X. Burda, C. R. Narayanan, M. A. El-Sayed, *Chem. Rev.* **2005**, *105*, 1025–1102.
[3] J. Zhang, X. Li, X. Sun, Y. Li, *J. Phys. Chem. B* **2005**, *109*, 12544–12548.
[4] Z. W. Pan, Z. R. Dai, Z. L. Wang, *Science* **2001**, *291*, 1947–1949.
[5] D. Li, J. T. McCann, Y. N. Xia, *Small* **2005**, *1*, 83–86.
[6] Y. N. Xia, P. D. Yang, Y. G. Sun, Y. Y. Wu, B. Mayers, B. Gates, Y. D. Yin, F. Kim, H. Q. Yan, *Adv. Mater.* **2003**, *15*, 353–389.
[7] T. D. Ewers, A. K. Sra, B. C. Norris, R. E. Cable, C. H. Cheng, D. F. Shantz, R. E. Schaak, *Chem. Mater.* **2005**, *17*, 514–520.
[8] H. G. Yang, H. C. Zeng, *Angew. Chem.* **2004**, *116*, 6056–6059; *Angew. Chem. Int. Ed.* **2004**, *43*, 5930–5933.
[9] X. Y. Chen, X. Wang, Z. H. Wang, X. G. Yang, Y. T. Qian, *Cryst. Growth Des.* **2005**, *5*, 347–350.
[10] Z. Q. Li, Y. Ding, Y. J. Xiong, Q. Yang, Y. Xie, *Chem. Commun.* **2005**, 918–920.
[11] Z. Q. Li, Y. Ding, Y. J. Xiong, Y. Xie, *Cryst. Growth Des.* **2005**, *5*, 1953–1958.
[12] X. W. Lou, H. C. Zeng, *J. Am. Chem. Soc.* **2003**, *125*, 2697–2704.
[13] M. S. Mo, J. C. Yu, L. Z. Zhang, S. K. A. Li, *Adv. Mater.* **2005**, *17*, 756–760.
[14] X. S. Fang, C. H. Ye, L. D. Zhang, J. X. Zhang, J. W. Zhao, P. Yan, *Small* **2005**, *1*, 422–428.
[15] F. Gao, Q. Y. Lu, S. H. Xie, D. Y. Zhao, *Adv. Mater.* **2002**, *14*, 1537–1540.
[16] Y. W. Jun, S. M. Lee, N. J. Kang, J. Cheon, *J. Am. Chem. Soc.* **2001**, *123*, 5150–5151.
[17] C. Coudun, J. F. Hochepicd, *J. Phys. Chem. B* **2005**, *109*, 6069–6074.
[18] M. H. Cao, X. Y. He, J. Chen, C. W. Hu, *Cryst. Growth Des.* **2007**, *7*, 170–174.
[19] J. Y. Chen, T. Herricks, M. Geissler, Y. N. Xia, *J. Am. Chem. Soc.* **2004**, *126*, 10854–10855.
[20] Q. Zhang, W. T. Yao, X. Y. Chen, L. W. Zhu, Y. B. Fu, G. B. Zhang, L. S. Sheng, S. H. Yu, *Cryst. Growth Des.* **2007**, *7*, 1423–1434.
[21] L. W. Qian, J. Zhu, Z. Chen, Y. C. Gui, Q. Gong, Y. P. Yuan, J. T. Zai, X. F. Qian, *Chem. Eur. J.* **2009**, *15*, 1233–1240.
[22] J. Yang, C. X. Li, X. M. Zhang, Z. W. Quan, C. M. Zhang, J. Lin, *Chem. Eur. J.* **2008**, *14*, 4336–4345.
[23] C. M. Zhang, J. Yang, Z. W. Quan, P. P. Yang, C. X. Li, Z. Y. Hou, J. Lin, *Cryst. Growth Des.* **2009**, *9*, 2725–2733.
[24] J. Yang, C. X. Li, Z. W. Quan, C. M. Zhang, P. P. Yang, Y. Y. Li, C. C. Yu, J. Lin, *J. Phys. Chem. C* **2008**, *112*, 12777–12785.
[25] A. W. Xu, Y. P. Fang, L. P. You, H. Q. Liu, *J. Am. Chem. Soc.* **2003**, *125*, 1494–1495.
[26] C. G. Hu, H. Liu, W. T. Dong, Y. Y. Zhang, G. Bao, C. S. Lao, Z. L. Wang, *Adv. Mater.* **2007**, *19*, 470–474.
[27] M. Y. Guan, F. F. Tao, J. H. Sun, Z. Xu, *Langmuir* **2008**, *24*, 8280–8283.
[28] X. Wang, Y. D. Li, *Angew. Chem.* **2002**, *114*, 4984–4987; *Angew. Chem. Int. Ed.* **2002**, *41*, 4790–4793.
[29] X. Wang, Y. D. Li, *Chem. Eur. J.* **2003**, *9*, 5627–5635.
[30] G. Chadeyron, R. Mahiou, M. El-Ghozzi, A. Arbus, D. Zambon, J. C. Cousseins, *J. Lumin.* **1997**, *72–74*, 564–566.
[31] Z. H. Li, J. H. Zeng, C. Chen, Y. D. Li, *J. Cryst. Growth* **2006**, *286*, 487–493.
[32] C. Mansuy, J. M. Nedelec, C. Dujardin, R. Mahiou, *Opt. Mater.* **2007**, *29*, 697–702.
[33] M. Ren, J. H. Lin, Y. Dong, L. Q. Yang, M. Z. Su, *Chem. Mater.* **1999**, *11*, 1576–1580.
[34] G. H. Pan, H. W. Song, X. Bai, Z. X. Liu, H. Q. Yu, W. H. Di, S. Li, L. Fan, X. Ren, S. Lu, *Chem. Mater.* **2006**, *18*, 4526–4532.
[35] Z. H. Li, J. H. Zeng, Y. D. Li, *Small* **2007**, *3*, 438–443.
[36] Z. G. Wei, L. D. Sun, C. S. Liao, J. L. Yin, X. C. Jiang, C. H. Yan, *J. Phys. Chem. B* **2002**, *106*, 10610–10617.
[37] H. W. Song, H. Q. Yu, G. H. Pan, X. Bai, B. Dong, X. T. Zhang, S. K. Hark, *Chem. Mater.* **2008**, *20*, 4762–4767.
[38] X. C. Jiang, L. D. Sun, W. Feng, C. H. Yan, *Cryst. Growth Des.* **2004**, *4*, 517–520.
[39] Y. P. Li, J. H. Zhang, X. Zhang, Y. S. Luo, S. Z. Lu, X. G. Ren, X. J. Wang, L. D. Sun, C. H. Yan, *Chem. Mater.* **2009**, *21*, 468–475.
[40] C. K. Lin, D. Y. Kong, X. M. Liu, H. Wang, M. Yu, J. Lin, *Inorg. Chem.* **2007**, *46*, 2674–2681.
[41] H. L. Zhu, L. Zhang, T. T. Zuo, X. Y. Gu, Z. K. Wang, L. M. Zhu, K. H. Yao, *Appl. Surf. Sci.* **2008**, *254*, 6362–6365.
[42] Y. H. Wang, C. F. Wu, J. C. Zhang, *Mater. Res. Bull.* **2006**, *41*, 1571–1577.
[43] J. Zhang, Z. G. Liu, J. Lin, J. Y. Fang, *Cryst. Growth Des.* **2005**, *5*, 1527–1530.
[44] G. Jia, M. Yang, Y. H. Song, H. P. You, H. J. Zhang, *Cryst. Growth Des.* **2009**, *9*, 301–307.
[45] J. Yang, C. M. Zhang, L. L. Wang, Z. Y. Hou, S. S. Huang, H. Z. Lian, J. Lin, *J. Solid State Chem.* **2008**, *181*, 2672–2680.
[46] J. Yang, C. M. Zhang, C. X. Li, Y. N. Yu, J. Lin, *Inorg. Chem.* **2008**, *47*, 7262–7270.
[47] Y. F. Xu, D. K. Ma, X. A. Chen, D. P. Yang, S. M. Huang, *Langmuir* **2009**, *25*, 7103–7108.
[48] B. R. Judd, *Phys. Rev.* **1962**, *127*, 750–761.
[49] G. Jia, K. Liu, Y. H. Zheng, Y. H. Song, M. Yang, H. P. You, *J. Phys. Chem. C* **2009**, *113*, 6050–6055.
[50] G. Jia, Y. H. Song, M. Yang, Y. J. Huang, L. H. Zhang, H. P. You, *Opt. Mater.* **2009**, *31*, 1032–1037.
[51] C. Feldman, *Phys. Rev.* **1960**, *117*, 455–459.
[52] Z. Y. Huo, C. Chen, D. R. Chu, H. H. Li, Y. D. Li, *Chem. Eur. J.* **2007**, *13*, 7708–7714.
[53] J. F. Liu, Y. D. Li, *J. Mater. Chem.* **2007**, *17*, 1797–1803.
[54] G. Jia, Y. H. Zheng, K. Liu, Y. H. Song, H. P. You, H. J. Zhang, *J. Phys. Chem. C* **2009**, *113*, 153–158.

Received: October 14, 2009
Published online: January 27, 2010

